Journal Pre-proof

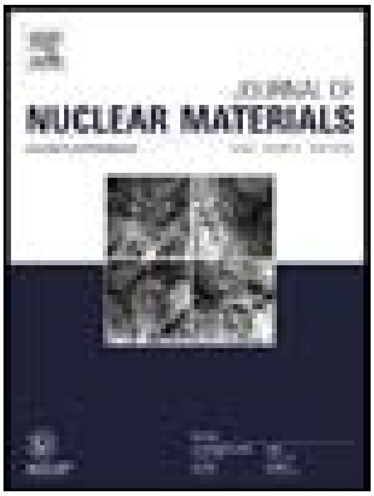

Small punch test size reduction to enable high flux irradiation

Ziwei Li , Dmitry Terentyev , Stefan Holmström , Thomas Pardoen

PII: S0022-3115(24)00592-0
DOI: https://doi.org/10.1016/j.jnucmat.2024.155491
Reference: NUMA 155491

To appear in: *Journal of Nuclear Materials*

Received date: 23 August 2024
Revised date: 25 October 2024
Accepted date: 30 October 2024

Please cite this article as: Ziwei Li , Dmitry Terentyev , Stefan Holmström , Thomas Pardoen , Small punch test size reduction to enable high flux irradiation, *Journal of Nuclear Materials* (2024), doi: https://doi.org/10.1016/j.jnucmat.2024.155491

Highlights:

- The methodology followed to establish the non-standard Small Punch test set-up is given.
- New SPT setup is developed for irradiation campaign using Chakrabarty model and FEA.
- The new SPT set-up shows reproducibility and interchangeability with standard set-up.

Small punch test size reduction to enable high flux irradiation

Ziwei Li[1, 2*], Dmitry Terentyev[1], Stefan Holmström[1], Thomas Pardoen[2,3]

[1]*SCK CEN, Boeretang 200, 2400 Mol, Belgium*
[2]*Université catholique de Louvain, 1438 Louvain-la-Neuve, Belgium*
[3]*WEL Research Institute, Avenue Pasteur, 1300 Wavre, Belgium*

Corresponding author: Ms Ziwei Li
E-mail: Ziwei.Li@sckcen.be

Abstract:

Screening and qualification of new nuclear materials with superior irradiation resistance requires expensive irradiation exposure and post-irradiation examination before consideration into industrial nuclear structural components. The development of miniaturized test methods is needed for enhanced cost/time efficient testing, while enabling comparative and robust material property estimation in a timely and high throughput manner. The Small Punch Test (SPT) is drawing much interest, especially since the publication of an European standard. Motivated by this standard, a new SP test sample geometry is proposed in order to reduce the material volume to be tested, hences increasing the number of samples that can be introduced in an irradiation rig is proposed. The modified sample diameter has been reduced from 8 to 5.35 mm. The qualification of this new design is described here together with a detailed description of the SPT setup modification as compared to the reference setup of the EN standard. Finite element analyses and a series of experiments have been conducted using both standard and reduced size SP samples to demonstrate that the modified test gives estimates of the basic mechanical properties with the same magnitude of error and validates the modified sample geometry for usage in irradiated material testing.

Key Words: Small Punch Test; Miniature specimen; mechanical properties

1. **Introduction**

The design and construction of future reactors like ITER[1,2] and DEMO [3,4] involve extreme technological challenges that heavily rely on advancements in engineering and applied sciences. In addition, the positive social perception of the nuclear energy generation as a safe green energy source is still progressing. Thus, the development and qualification of the structural materials to be used in the future nuclear installations require rigorous demonstration of their mechanical properties, including performance during service under neutron irradiation, to satisfy current design safety limits[5]. Large industrial engineering projects [6,7], as well as European projects like the INNUMAT [8] under which this work is conducted, are ongoing to produce and validate new and enhanced variants of classical materials [9–11] with dedicated microstructure and chemistry targeting the reduction of the detrimental impact caused by neutron irradiation [12]. Irradiation experiments conducted at material test reactors (MTRs) are performed to expose materials to the selected levels of irradiation damage while being able to host samples with dimensions complying to the requirements of the standards. The validation, screening and qualification of irradiated samples is one of the steps needed to raise the technological readiness level (TRL) of the specific material's solutions and components. Since irradiation in MTRs is extremely expensive, even for small quantities or volumes, the cost/time efficiency is of major importance. Small Specimen Testing Techniques (SSTT) [13,14] are being developed and studied for use in post-irradiation testing in order to minimizing the amount of material to be irradiated.

The Small Punch Test (SPT) [15,16], in particular, is currently receiving significant interest from the nuclear field owing to recent publication of standardized test methods, with the capability to acquire robust tensile property estimates with a small specimen volume and a fast experimental procedure.

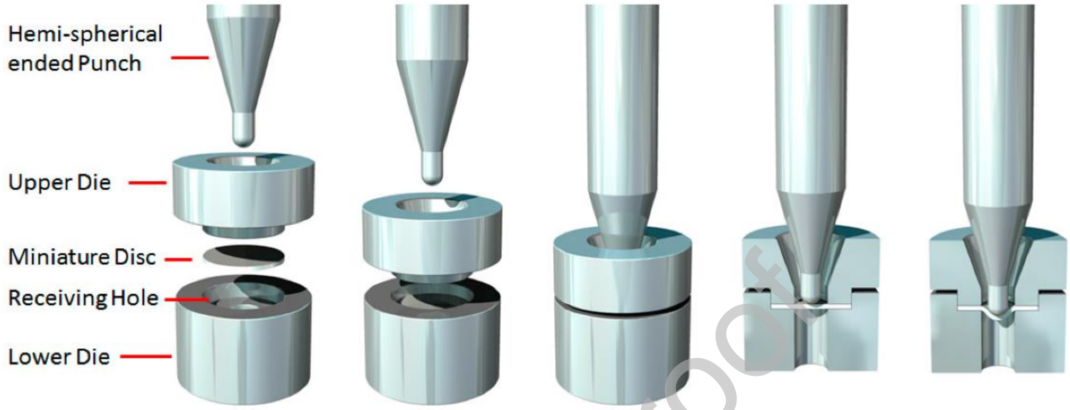

Fig. 1. Illustration of Small Punch Test setup and basic stages of the test [17].

A typical SPT set-up [18], shown in Fig. 1, consists of an upper and lower die to clamp the sample. A hemispherical tip puncher (or flat puncher together with a ball) is placed above the specimen and displaced towards the specimen during the experiments. For post-irradiation materials analysis, SPT has already proven to be effective in determining the Ductile to Brittle Transition Temperature (DBTT) [19–22]. Moreover, several successful campaigns have been made to characterize the irradiation effect on tensile properties [23–25]. For instance, the analysis of mechanical properties of ferritic/martensitic steel T91 before and after irradiation show that the effect of irradiation on yield stress can be determined by SPT, providing the quantitative values for the irradiation hardening [23]. The post-irradiation analysis (testing and microscopy of tested samples) of another classical steel used in power generation installations, 2.25Cr1Mo, irradiated at ~400 °C, indicated that SPT is not only able to quantify the irradiation-induced embrittlement effect, but could also successfully reveal the proper fracture mechanism by studying the SPT fracture surface [22]. The SPT technique has also been utilized for the assessment of proton irradiated bombarded austenitic stainless steel SS316L thin foil samples, showing also, in this case, the capability of capturing the ductile to brittle material transition as a function of the increasing irradiation damage [25].

The EN small punch standard EN10371[16], published in 2021, gives a detailed description of the standardized test setup, sample dimensions, experimental procedure, and post-processing method. The SPT has therefore gained further interest for use in the support of design and as a tool for the long term operation (LTO) management. The newly revised RCC-MRx design code [5] for the construction of nuclear installations includes a probationary rule section that permits the use of SPT for life extension purposes and as 'supporting' data. This naturally opens new routes and perspectives for the application of the SPT in the extraction of mechanical properties of nuclear materials.

The current sample dimensions covered by the standard include 8 mm and 3 mm diameter (Φ) specimens with a thicknesses of 0.5 and 0.25 mm, respectively. However, the application of 8 mm diameter sample is not optimal for the screening of the irradiation effects when it comes to development and optimization of new materials, as a significant quantity of material might be needed for this purpose. On the other hand, the testing of3 mm diameter sample involves several challenges when handled in hot cell environment. First of all, given the need for material screening, proper labeling and identification of the sample are crucial for the tracing before and after irradiation. However, the small size of 3 mm diameter samples makes labeling difficult and identification in hot lab even more challenging. Moreover, the Φ = 1 mm puncher applied on Φ = 3 mm SPT can only be achieved with ceramic balls as the manufacturing of a Φ = 1 mm metallic puncher is difficult , and using ceramic balls in hot lab environment with manipulators adds more complexity. Therefore, in order to optimize the experimental throughput, a new SPT sample size with a diameter of 5.35 mm and the adaptation of the SPT setup is presented in this work. The new SPT sample geometry has a diameter of 5.35 mm and a thickness of 0.4 mm. With the reduced sample size, the number of specimens that can be accommodated in one single irradiation capsule is doubled. The thickness of the sample was determined during the optimization process to reproduce the stress-strain behavior of the specimen with Φ = 8 mm. The test setup dimensions that required alteration to accommodate the new sample forced to change the diameter of the receiving hole from 4 mm to 3.2 mm. The optimum punch diameter is also changed from 2.5 mm to 2 mm for neutron irradiation campaign use. In this work, finite element analyses (FEA) and a series of SPTs are conducted for both the standard and the modified SPT samples to (1) optimize the SP sample geometry and then to (2) validate the new sample geometry and SPT setup modifications in comparison to the standard sample and test setup. The experiments used for this comparative study are performed using the reduced activation ferritic–martensitic (RAFM) structural steel EUROFER97, and the experimental tests include both SPT and uniaxial tensile tests. Uniaxial tensile tests are performed to both (1) validate the SPT results and (2) for derivation of the FEA parameters needed in the SPT simulations.

2. Methods

In this section, a thorough description of the methodology for developing the new geometry of the SP sample and test setup is described first. This will be followed by the introduction of the FEA applied to determine the most suitable geometry for the miniaturized SPT. Finally, the experimental program, including both SPTs and uniaxial tensile tests, are reported to validate the newly-proposed test sample and test setup.

2.1. Miniaturization strategy for SPT

As stated in the introduction, the primary reason behind the development of the new miniaturized sample geometry is to limit the material needed and the irradiation costs for the assessment of the properties of nuclear structural materials. Therefore, in order to maximize the number of samples that can be loaded into an irradiation compartment while keeping the acceptable operability in hot cell environment (i.e. handling with two finger manipulators), a sample diameter of 5.35 mm was considered optimum. The choice of such geometry enables the usage of high flux irradiation positions in MTRs such as HFIR, BR2 or HFR, where the irradiation positions are familiarly called "RABBIT capsules". This space is limited to about 12-14 mm in diameter [26]. Thanks to the proposed miniaturization, two stacks of samples can be loaded, as illustrated schematically in Fig. 2, which shows the irradiation holder and sample positions for the RABBIT capsule in the BR2 reactor.

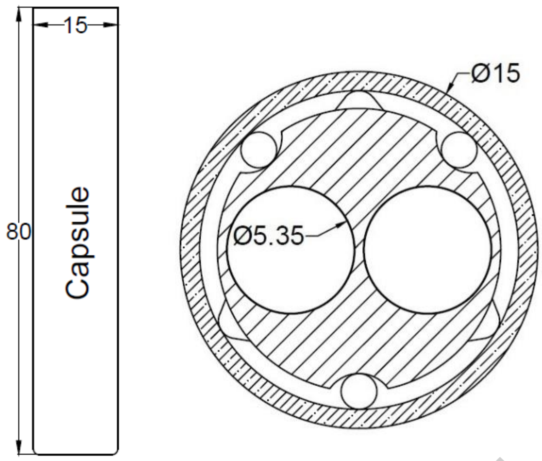

(a) (b)

Fig. 2. (a) Front-view of an irradiation RABBIT capsule; (b) Cross section drawing of an irradiation capsule with 2 stacks of Φ = 5.35 mm SPT samples (Units: mm).

Due to the change of the sample diameter (*D*s), the SPT sample thickness and the test-setup dimensions have been reconfigured to perform as similarly as possible to the Φ = 8 mm specimen in terms of the stress-strain response. The to-be-determined geometrical parameters include: sample thickness (*h*); radius of punch tip (*r*); radius of receiving hole (*R*). The chamfer length of the test set-up (*L*) for the Φ = 5.35 mm SPT sample was chosen to remain equal as 0.2 mm, since a smaller chamfer would be extremely difficult to fabricate with high accuracy. For this optimization exercise certain criteria should be met in order to ensure the success of the miniaturization as compared to the standard Φ = 8 mm test configuration.

The first criterion to follow is to have the stress state for the miniaturized Φ = 5.35 mm SP geometry as similar as possible to the standard Φ = 8 mm. The Chakrabarty membrane stretch model [27] was used to guide. In the Chakrabarty model, the force to membrane stress ratio (F/σ) can be calculated as:

$$\frac{F}{\sigma} = 2\pi r h^* \sin^2 \theta_0 \, , \tag{1}$$

$$h^* = h\left(\frac{1+\cos\theta_0}{1+\cos\theta}\right)^2 , \tag{2}$$

where r is the radius of punch tip, h^* is the sample thickness at the contact boundary, h is the initial thickness, θ is the angle at the boundary, while θ_0 is the angle of contact, as described in Fig. 3(a). The membrane stress is then converted into engineering stress by dividing it by the relation $(1+h/r)$. Therefore, a consistent stress state can only be achieved when the relation $(1 + h/r)$ remains unchanged[29].

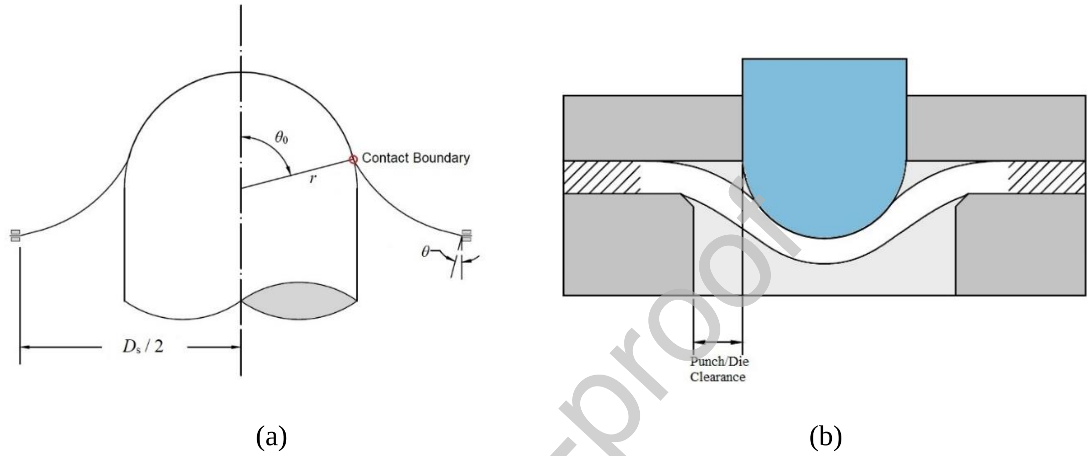

Fig. 3. (a) Geometry of deformation based on Chakrabarty membrane stretch model [27]*; (b) Illustration of punch/die clearance and clamping surface(shadowed area).*

The second criterion is to achieve deformation level (local strain) that would be representative of the standard Φ = 8 mm sample. This can be accomplished once the two following test-setup geometry parameters are optimized. The first parameter is the punch/die clearance. The clearance, as shown in Fig. 3(b), should not be too large otherwise there will not be enough clamping area for the samples, nor too small so that there would be thinning or even tearing in the samples. The second parameter is the clamping surface area (shadowed area in Fig. 3(b)), which is the area where the upper die and lower die are in contact with the specimen. The clamping surface area should not be too small to let the samples slip and sink into the receiving hole.

The steps followed to develop the new test rig geometry is as follow: (1) a set of geometries is proposed at first based on the first criterion, which is to have a $(1+h/r)$ ratio equal to 1.4, same as the standard Φ = 8 mm sample. (2) Finite element analyses are carried out on the proposed geometries in the first step for further inspection of the deformation process during tests to check if the second criterion is met. The proposed sets of geometries in this study are given in Table 1.

Table 1 Proposed geometries for new miniaturized SPT rig.

Label	Sample diameter D_s [mm]	Sample thickness h [mm]	Punch radius r [mm]	Receiving hole radius R [mm]
Standard	8	0.5	1.25	2
Design_1	5.35	0.5	1.25	2
Design_2	5.35	0.5	1.25	1.9
Design_3	5.35	0.5	1.25	1.8
Design_4	5.35	0.4	1	2
Design_5	5.35	0.4	1	1.8
Design_6	5.35	0.4	1	1.6

2.2. Finite element analyses (FEA)

FEA have been carried out using the commercial FE code ABAQUS [28]. The model, described in Fig. 4, is a 2D axisymmetric model owing to the rotational symmetry of the experimental set-up. The model consists of three parts: the puncher, the dies, and the small punch specimen. The puncher and the dies are modelled as rigid bodies interacting with the specimen surface. The friction coefficient in the contact region is chosen as equal to 0.2 as proposed in [29]. The specimens were modelled using CAX4R elements. A maximum vertical displacement of -2.5 mm is progressively applied to the puncher. The dies are constrained in all directions. The material properties were extracted from the uniaxial tensile tests of EUROFER 97 at 22°C and 300°C reported in Section 2.3.2. The hardening laws are shown in Fig. 5 and the elastic properties are given in Table 2. The hardening law after necking is determined based on the method described in [30]. The material properties at 22°C are used to determine the suitable design for new miniaturized SPT test rig, while both material properties at 22°C and 300°C are needed to further validate the chosen design.

Simulations were repeated with different mesh refinements during a preliminary analysis in order to ensure converged mesh-independent responses. All the geometries presented in the last section have been simulated. The results will be presented in Section 3.1.

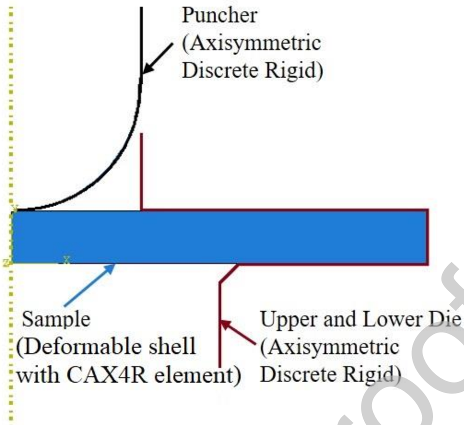

Fig. 4. Illustration of the finite element model used for Simulating the SPT.

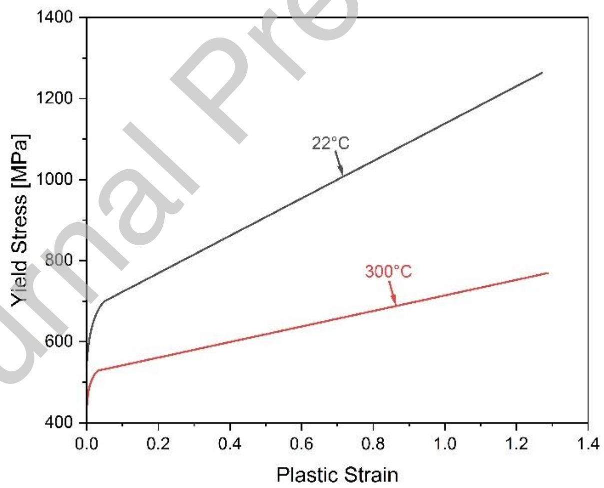

Fig. 5. Hardening law of EUROFER 97 Batch 3 ID48 at 22°C and 300 °C.

Table 2 Elastic properties of EUROFER 97 Batch 3 ID48 at 22°C and 300 °C.

Temperature [°C]	Young's Modulus [GPa]	Poisson's Ratio
22	207	0.3
300	193	0.3

2.3. Experimental setup

In order to validate the selected miniaturized test geometry based on the material properties of EUROFER97, a set of tests, including the newly proposed Φ = 5.35 mm SPT, standard Φ = 8 mm SPT, and uniaxial tensile tests, has been carried out at 22°C and 300°C. EUROFER97 is a Reduced Ferritic-Martensitic (RAFM) steel that has been developed to avoid long-term radiative decay and will be applied as the main structural material for fusion reactors. The EUROFER97 in this study belongs to Batch 3 and the samples are cut from the plate identified as "ID 48". Detailed description of the test matrix is given in Table 3.

Table 3 Test matrix.

Material	Test Type / samples per test condition	Temperature [°C]
EUROFER 97 Batch 3 ID 48	uniaxial tensile test / 3 Standard Φ = 8 mm SPT / 3 Φ = 5.35 mm SPT / 3	22, 300

2.3.1. SPT procedures

Small Punch tests for both standard Φ = 8 mm SPT and newly proposed Φ = 5.35 mm SPT were performed accordingly to the EN10371:2020 standard test procedure [16]. The test setup for both geometries is given in Fig. 6. The samples were cut by Electric Discharge Machining (EDM) and then polished. After the polishing, the thickness was measured using a micrometer at six different positions for each sample to ensure precision, as required by the standard. The as-measured thickness of the samples used in this work is given in Table 4. Please note that specimens labeled with 'S' represent standard Φ = 8 mm samples, while those labeled with 'M' represent miniaturized Φ = 5.35 mm samples. It is found that yet being close to 0.5 mm and 0.4 mm, some of the thicknesses are not within the very strict tolerance prescribed by the standard 5 μm for the 0.5 mm thick sample, and 4 μm for the 0.4 sample. However, the differences between maximum thickness and minimum thickness of each sample are not larger than 8 μm. This indicates a good level of flatness of the samples, therefore, the deviation from the standard in sample thickness is considered acceptable.

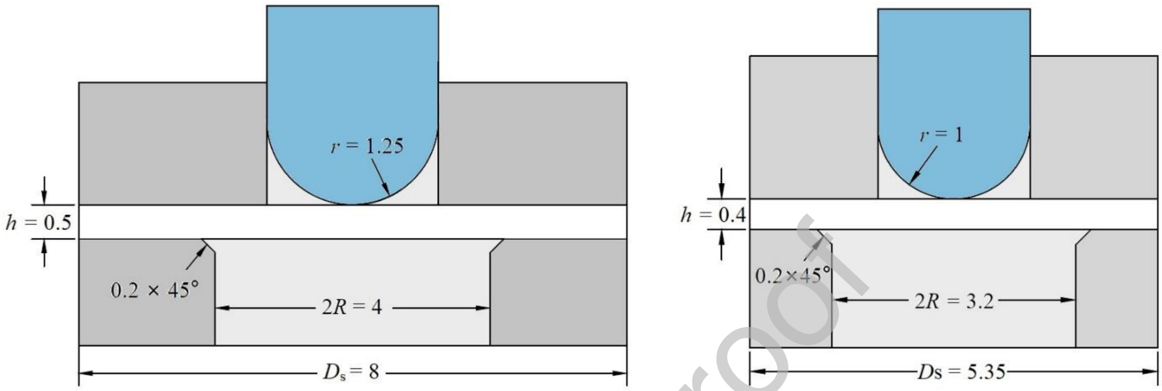

(a) (b)

Fig. 6. SPT set-up and dimensions: (a) standard Φ =8 mm SPT; (b) newly-proposed Φ = 5.35 mm SPT (Units: mm).

Table 4 SPT specimen dimensions

Test Temperature [°C]	Label	Sample diameter D_s [mm]	Average Specimen thickness h_0 [mm]	Maximum specimen thickness h_{max}[mm]	Minimum Specimen thickness h_{min} [mm]
22	22S1	8	0.499	0.502	0.494
	22S2		0.505	0.506	0.503
	22S3		0.511	0.513	0.507
300	300S1	8	0.515	0.518	0.510
	300S2		0.518	0.519	0.517
	300S3		0.521	0.521	0.520
22	22M1	5.35	0.396	0.397	0.395
	22M2		0.398	0.401	0.394
	22M3		0.412	0.413	0.411
300	300M1	5.35	0.414	0.415	0.412
	300M2		0.418	0.419	0.417
	300M3		0.423	0.426	0.419

The tests were performed on an Instron universal test bench (model: 8801). The displacement rate of the puncher was set equal to 0.2 mm/min. For the elevated temperature tests, a thermocouple was placed in the receiving hole in contact with the lower die just below the specimen. A soaking time of 30 min was applied to stabilize the temperature before the tests start. The displacement was measured using LVDT (linear variable differential transformer) attached to the pull rod. The load was measured by the calibrated and certified load cell with the maximum load of 5 kN. No pre-load was applied. The tests were continued beyond the maximum load until the load dropped below 80% of its maximum value. Before processing the data, the stiffness of load-line was measured to establish the compliance correction.

Then, the displacement measured during the experiments via LVDT attached to the pull rod is corrected using the machine compliance as following:

$$v = v_{ref} - F(v_{ref})C_p, \tag{3}$$

where v_{ref} is the measured displacement, C_p is the compliance coefficient and $F(v_{ref})$ is the force measured at the measured displacement.

The ultimate tensile strength (UTS) and yield stress (YS) were extracted from the force-displacement curves in order to validate the newly-proposed Φ = 5.35 mm SPT geometry in terms of extracting tensile properties. The tri-linear method given in the standard is used to determine YS since the displacement is measurand in this test configuration, while the maximum force method is used to extract UTS. A thorough description on the process to extract YS and UTS is given in Appendix A.

2.3.2. Uniaxial tensile testing

Standard uniaxial tensile tests were performed using an Instron universal test bench (model: 8801) in order to determine the tensile properties of EUROFER97 at room temperature and at 300 °C, for further comparison with the results extracted from SPT. The geometry of the tensile specimen is given in Fig. 7. The tests were carried out in a static tensile mode with a constant crosshead speed of 0.2 mm/min. For the tests at elevated temperature, 30 min soaking time was applied and the temperature was controlled via a thermocouple. The load was measured by the load cell and the displacement correspondeds to the displacement of the crosshead. The analyses of the experimental data and the extraction of the mechanical tensile properties were carried out based on ASTM E8 standard [31].

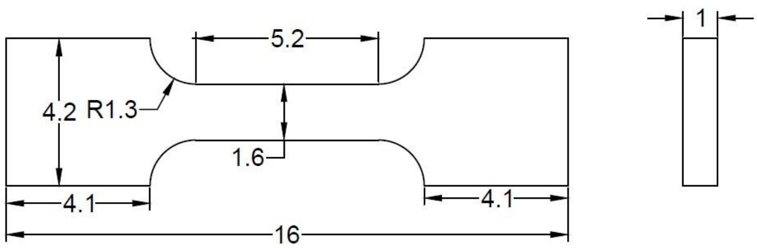

Fig. 7. Dimensions of Tensile samples (Units: mm).

3. Results

In this section, at first, we present the results of the FEA which was used to optimize the SPT setup for Φ = 5.35 mm specimen. Then, the experimental results for both SPTs and uniaxial tensile tests are given and discussed in order to validate the applicability of the miniaturized SPT specimen.

3.1. FEA results

All six designs given in Table 1 alongside with the standard Φ = 8 mm SPT set-up were modelled. The FE simulated force-displacement curves are presented in Fig. 8. In order to check if the sample deformation among all designed models can meet the criterion mentioned in Section 2.1, the deformed configuration of all designed SP test set-up at maximum force are in Fig. 9. The distribution of PEEQ (equivalent plastic strain) at maximum force is given in Fig. 10, the PEEQ distribution is only shown for a half of the specimen cross-section.

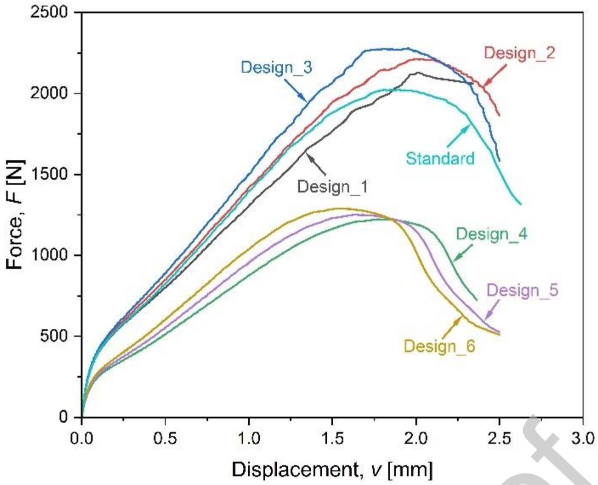

Fig. 8. Force-Displacement curves predicted by FEA for the 6 designs.

Fig. 9 shows that Design_1, Design_2 and Design_4 are not suitable for the miniaturized SP test setup, because the clamping surface area is not sufficient to maintain the sample and can cause invalid results due to sliding or bending out of position during the experiment. The area indicated by the red circles in Fig. 9(b), (c) and (d) shows that the clamped area has a tendency to bend upwards, which is another sign of insufficient constraint. For the other three designs, the deformation profile is similar to the standard Φ = 8 mm sample. However, based on Fig. 10, when the deformation is quantitatively described using PEEQ, only Design_6 is found to undergo a level of plastic strain similar to the standard Φ = 8 mm geometry at maximum force, while Design_3 exhibits smaller plastic strains and Design_5 exhibits higher plastic strains. This indicates that the test setup Design_6 meets the criterion of achieving a deformation field representative of the standard Φ = 8 mm sample. Moreover, when calculating the punch/die clearance to sample thickness ratio ($(R\text{-}r)/h$), Design_6 has the same ratio as the standard Φ = 8 mm SP test rig, equal to 1.5. This naturally shows that the punch/die clearance of Design_6 is suitable for this newly-proposed SPT sample. In summary, Design_6, which has a sample diameter of 5.35 mm, a sample thickness of 0.4 mm, a punch radius of 1 mm, and a receiving hole radius of 1.6 mm is the most suitable test set-up for the dedicated Φ = 5.35 mm SPT configuration, and will be further validated through comparison experiments with standard Φ = 8 mm SP tests.

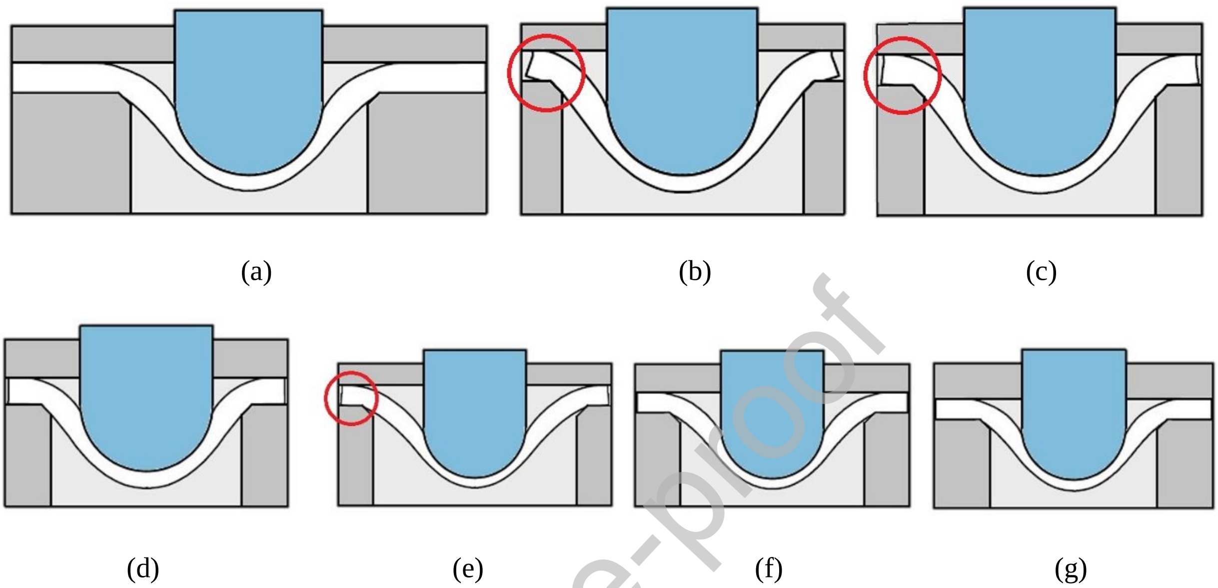

Fig. 9. Deformed configuration at maximum force: (a) standard Φ = 8 mm Small Punch test set-up; (b) Design_1; (c) Design_2; (d) Design_3; (e) Design_4; (f) Design_5; (g) Design_6.

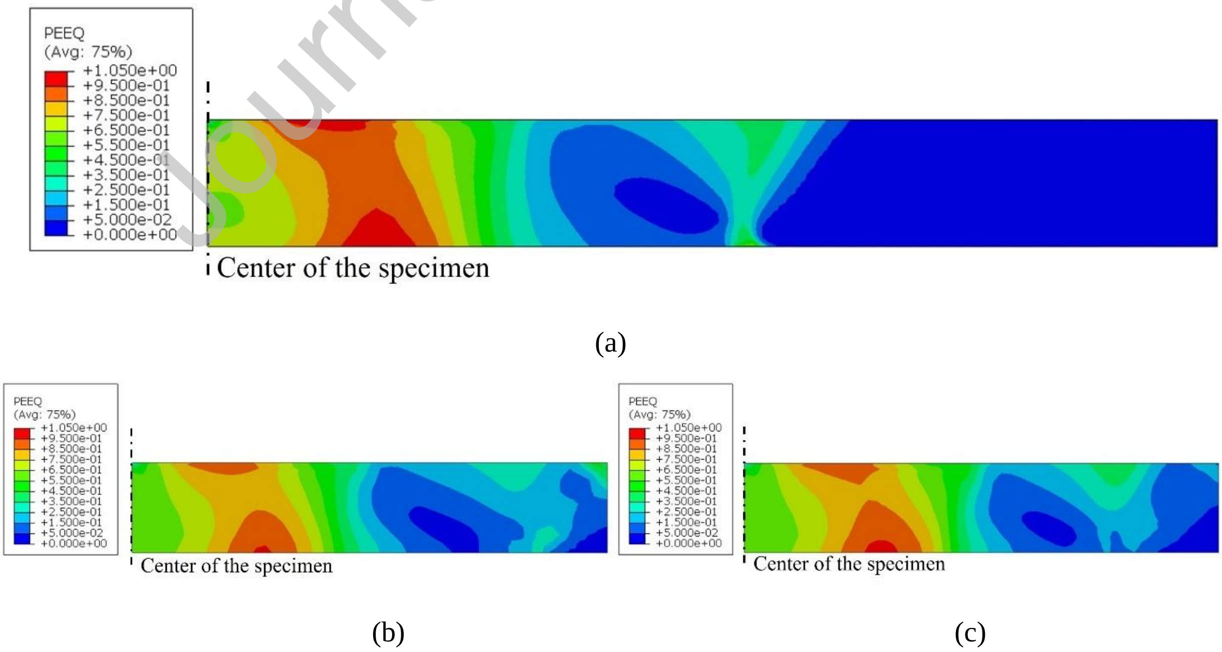

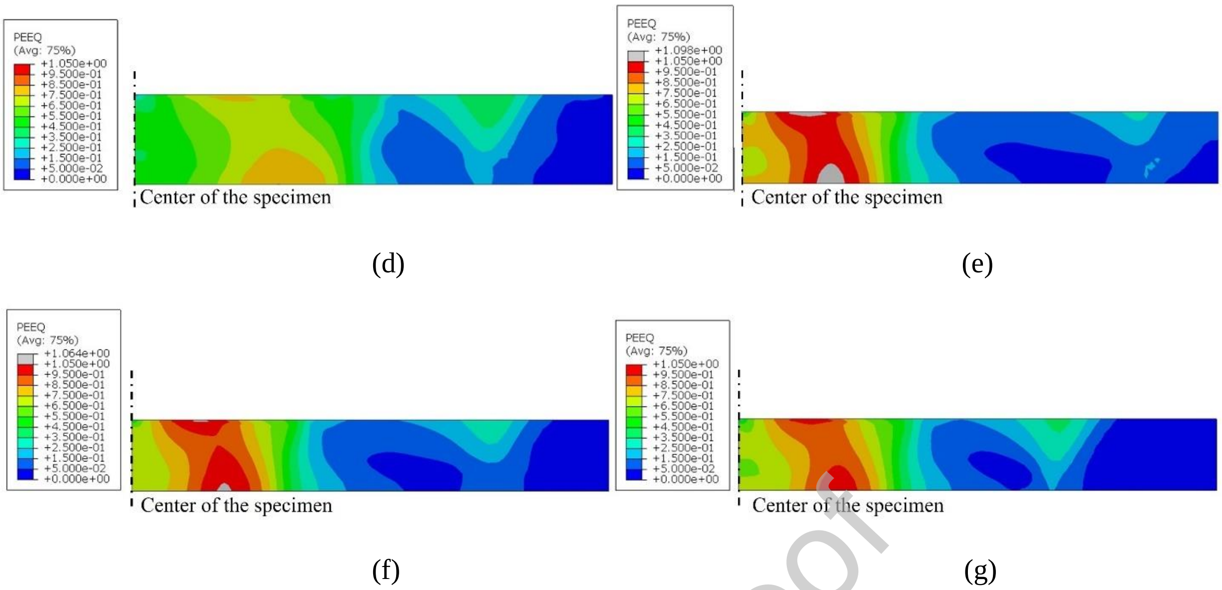

Fig. 10. Distribution of PEEQ (Equivalent Plastic Strain) at maximum force shown on half of the cross section: (a) standard Φ = 8 mm Small Punch test set-up; (b) Design_1; (c) Design_2; (d) Design_3; (e) Design_4; (f) Design_5; (g) Design_6.

3.2. Uniaxial tensile test results

The engineering stress-strain curves obtained from tensile experiments are given in Fig. 11, and a summary of the tensile properties (including yield stress, ultimate tensile strength, uniform elongation, total elongation and reduction of area) is given in Table 5. The figures presented in Table 5 are the average values of the three tests performed at each test temperature.

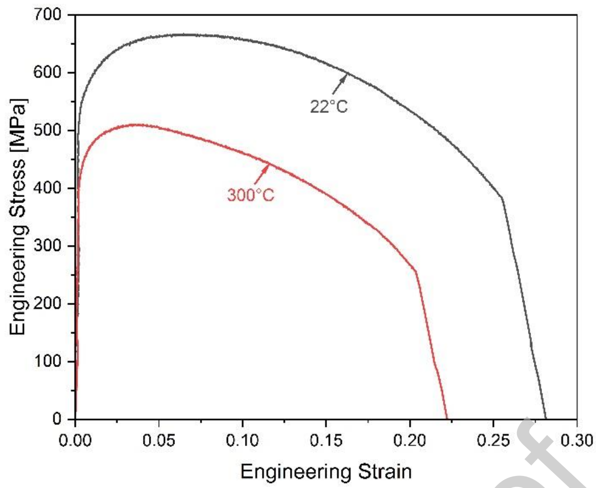

Fig. 11. Engineering stress-strain curves for EUROFER97 Batch 3 ID 48 at 22°C and 300°C.

Table 5 Tensile properties including yield stress, ultimate tensile strength, uniform elongation, total elongation, and reduction of area of EUROFER97 Batch 3 ID 48 at 22 and 300°C.

Test Temperature [°C]	Yield Stress, $R_{p0.2}$ [MPa]	Ultimate Tensile Strength, R_m [MPa]	$R_m / R_{p0.2}$	Uniform Elongation [%]	Total Elongation [%]	Reduction of Area [%]
22	538	660	1.23	6.2	26.3	73
300	444	511	1.15	3.2	20.2	72

As expected, Table 5 indicates that the yield stress and ultimate tensile strength are both smaller at 300 °C. Similarly, the uniform elongation, indicating the strain hardening capacity, decreases as the temperature rises. The same conclusion can also be drawn based on the reduction of the ratio between ultimate tensile strength and yield stress.

3.3. Small punch test results

3.3.1. Compliance-corrected force-displacement curves

The compliance–corrected force displacement curves for both types of specimen dimensions are presented in Fig. 12. To quantitively determine the reproducibility of the force-displacement curves, several key values have been obtained and shown in Table 6 as well. These values include F_m (maximum force), v_m (displacement at maximum force), and F_e (elastic-plastic transition force), since these are parameters required to obtain yield stress and ultimate tensile strength. The method used to extract F_e is given in Appendix A.

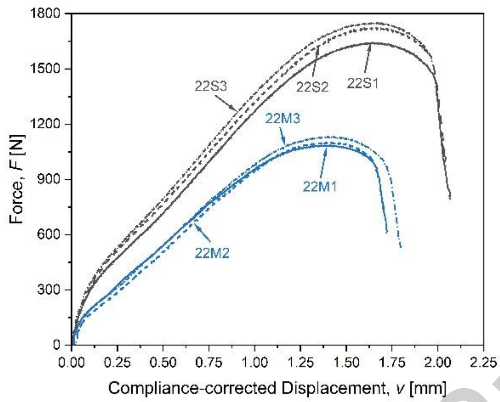

(a)

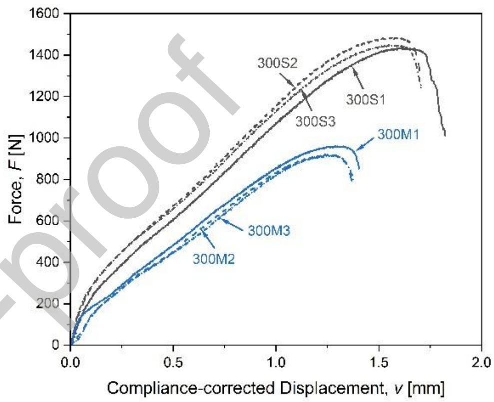

(b)

Fig. 12. Compliance-corrected force-displacement curves for both SPT set-ups: (a)22°C; (b) 300°C.

Table 6 F_m, v_m and F_e determined using compliance-corrected force-displacement curves.

Test Label	Average specimen thickness h_0 [mm]	F_m [N]	v_m [mm]	F_e [N]
22S1	0.499	1644	1.64	325
22S2	0.505	1724	1.71	338
22S3	0.511	1751	1.62	359
22M1	0.396	1087	1.41	145
22M2	0.398	1102	1.42	129
22M3	0.412	1133	1.40	157
300S1	0.515	1435	1.62	254
300S2	0.518	1485	1.59	298
300S3	0.521	1448	1.55	283
300M1	0.414	961	1.29	126

300M2	0.418	920	1.26	187
300M3	0.423	916	1.28	162

Despite the small differences in the test response observed in Fig. 12, which may be caused by small differences in specimen thickness, both SP tests show a good reproducibility. The same conclusion can be drawn from Table 6, which summarizes the F_m, v_m and F_e values. Both F_m and F_e increase with increasing thickness. For v_m, the thickness has negligible or no effect, and the variation of v_m within the same test condition is less than 0.1 mm (< 2.5 % of the theoretical thickness). It is important to note that the location of v_m is sensitive to both friction (necking location) and the stability of the LVDT signal, especially if the force-displacement curve is very flat at the end part of the test. Moreover, Table 6 also shows that as temperature increases, for both standard Φ = 8 mm and Φ = 5.35 mm SP tests, F_m, v_m and F_e all decrease. Thus, one can conclude that the results obtained using Φ = 5.35 mm sample follow the same trend as the one obtained using the standard sample size.

The interchangeability between both types of specimen geometry is discussed based on the Chakrabarty membrane stretch model. Based on the Chakrabarty model, the force-displacement curves of the Φ = 5.35 mm SPTs can be converted to the force-displacement curves of the Φ = 8 mm SPTs. The procedure is the following: first, the relationships between force to stress ratio and displacement for both test geometries are calculated according to Equation (1) and (2) and the results are plotted in Fig. 13(a).

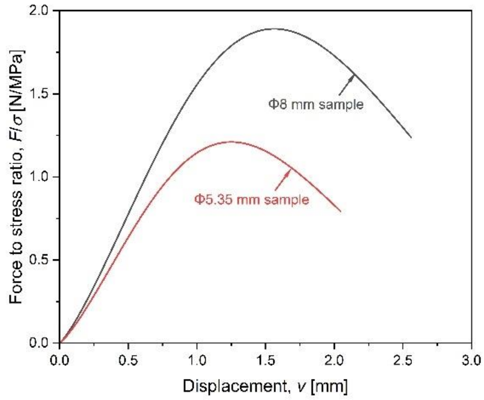

(a)

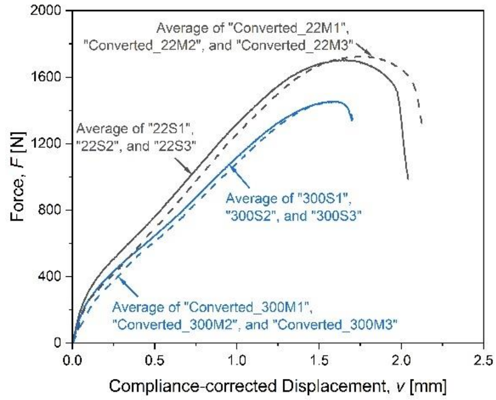

(b)

Fig. 13. (a) Relationship between force to stress ratio and displacement calculated based on Chakrabarty model for standard Φ8mm and Φ5.35 mm SPT; (b) Comparison between 8 mm SPT force-displacement curves and the converted 5.35 mm test results

Then, conversion ratios for both force to stress ratio and displacement can be calculated, these are given as:

$$\frac{\left[\frac{F}{\sigma}\right]_8}{\left[\frac{F}{\sigma}\right]_{5.35}} = 1.5625, \tag{4}$$

$$\frac{v_8}{v_{5.35}} = 1.25. \tag{5}$$

Finally, the ratios are applied to the force-displacement curves of Φ = 5.35 mm SPTs, and the results are given in Fig. 13(b). For simplicity, we provide the average of curves extracted from the same test condition.

Fig. 13(b) shows that the conversion leads to a limited error between the converted-Φ8 mm and the actual Φ = 8 mm tests. This can be caused by the use of theoretical sample thickness and the neglect of friction in the Chakrabarty model. Despite the limited error, the conclusion still holds that same material response can be observed during the experiments for standard 8 mm sample and newly-proposed 5.35 mm sample and that the interchangeability between both test set-ups is demonstrated.

3.3.2. Extraction of YS and UTS

After the tests, YS and UTS are also extracted based on the procedures described in Appendix A. The results are given in Table 7 and Table 8. The '$Std/YS_{Tensile}$' is calculated based on:

$$\overline{YS_{SPT}} = \frac{[YS_{SPT}]_1 + [YS_{SPT}]_2 + [YS_{SPT}]_3}{3}, \quad (6)$$

$$\frac{Std}{YS_{Tensile}} = \frac{\sqrt{\frac{([YS_{SPT}]_1 - \overline{YS_{SPT}})^2 + ([YS_{SPT}]_2 - \overline{YS_{SPT}})^2 + ([YS_{SPT}]_3 - \overline{YS_{SPT}})^2}{3}}}{YS_{Tensile}}, \quad (7)$$

where $YS_{Tensile}$ is the yield stress from the uniaxial tensile tests, the $[YS_{SPT}]_1$, $[YS_{SPT}]_2$, and $[YS_{SPT}]_3$ are yield stress extracted from the three SP tests, one per test condition respectively. Moreover, the '$Deviation/YS_{Tensile}$' is calculated according to:

$$\frac{Deviation}{YS_{Tensile}} = \frac{\sqrt{\frac{([YS_{SPT}]_1 - YS_{Tensile})^2 + ([YS_{SPT}]_2 - YS_{Tensile})^2 + ([YS_{SPT}]_3 - YS_{Tensile})^2}{3}}}{YS_{Tensile}}, \quad (8)$$

The '$Std/YS_{Tensile}$' ratio here represents the scatter of the YS calculated from the SP test, while the '$Deviation/YS_{Tensile}$' stands for the accuracy of the YS values calculated from the SP test with respect to the YS value calculated from tensile tests. The same relationships are also applied to '$Std/UTS_{Tensile}$' and '$Deviation/UTS_{Tensile}$' respectively.

Table 7 shows that the standard Φ = 8 mm SPTs overestimate the yield stress for both temperatures using the standard correlation coefficient, while the newly proposed Φ = 5.35 mm SPTs generally gives a lower estimation of the yield stress. The discrepancy of the identified yield stress by SPT can be caused by the inappropriate value of the empirical coefficient $\beta_{Rp0.2}$ taken from the standard. In other words, the coefficient given in the standard may not be applicable to the EUROFER97 material. The procedure described in Appendix A to determine the $\beta_{Rp0.2}$ for Φ = 5.35 mm SPTs is theoretical and does not take friction and the difference between average sample thickness and theoretical specimen thickness into account. Despite this discrepancy, the similarity in the '$Std/YS_{Tensile}$' values suggests that the yield strength measurements are comparably repeatable for both types of specimens. Moreover, the 'Deviation/$YS_{Tensile}$' calculated from the standard Φ = 8 mm SPTs are slightly larger than for the miniaturized sample. This suggests that the newly proposed Φ = 5.35 mm SPTssetup provides a yield stress within the same magnitude of accuracy as the standard Φ = 8 mm SPTs.

Table 7 YS (Yield Stress) obtained from SPT.

Test Type	Test Temperature [°C]	Label	YS-Tensile [MPa]	$F_e/(h_0^2)$ [MPa]	YS-SPT [MPa]	Std/ $YS_{Tensile}$ [%]	Deviation / $YS_{Tensile}$ [%]
standard Φ8 mm	22	22S1	538	1306	625	4	+20
		22S2		1321	633		
		22S3		1398	670		
Φ5.35 mm	22	22M1	538	922	442	5	-19
		22M2		849	407		
		22M3		992	475		
standard Φ8 mm	300	300S1	444	960	460	7	+14
		300S2		1110	532		
		300S3		1044	500		
Φ5.35 mm	300	300M1	444	842	403	10	+11
		300M2		1070	513		
		300M3		903	433		

Table 8 shows that both SPTs underestimate the UTS at 22°C, while the SP results overestimate the UTS at 300°C. The deviations can be related to the use of a theoretical value of β_{Rm}. The theoretical β_{Rm} value is taken from Chakrabarty model which neglects friction. However, both of them give a stable UTS prediction with standard deviation less than 5% of the UTS calculated from the tensile test. Moreover, the predictions made by both SPTs give similar results, and a similar value of $F_m/(h_0 v_m)$ is also achieved. Besides, both test setups exhibits similar value of 'Deviation/$YS_{Tensile}$', indicating comparable accuracy of the acquisition of the UTS value. Therefore, it can be concluded that the newly-proposed Φ = 5.35 mm SPT setup is interchangeable with the standard Φ = 8 mm SPT set-up and can produce repeatable results in terms of extracting the UTS.

Table 8 UTS (Ultimate Tensile Strength) obtained from Small Punch tests.

Test Type	Test Temperature [°C]	Label	UTS-Tensile [MPa]	$F_m/(h_0 v_m)$ [MPa]	UTS-SPT [MPa]	Std/ $UTS_{Tensile}$ [%]	Deviation / $UTS_{Tensile}$ [%]
standard Φ8 mm	22	22S1	660	2006	593	3	-9
		22S2		1997	593		
		22S3		2129	633		
Φ5.35 mm	22	22M1	660	1944	574	2	-12
		22M2		1944	575		
		22M3		2036	602		
standard Φ8 mm	300	300S1	511	1723	514	2	+4
		300S2		1800	538		
		300S3		1797	538		
Φ5.35 mm	300	300M1	511	1800	538	2	+3
		300M2		1746	524		
		300M3		1696	510		

4. Discussion

The discussion starts with a comparison between SP finite element model and experimental test. First of all, the force-displacement curves from FEA are compared with the force-compliance-corrected displacement curves from the experiments in Fig. 14.

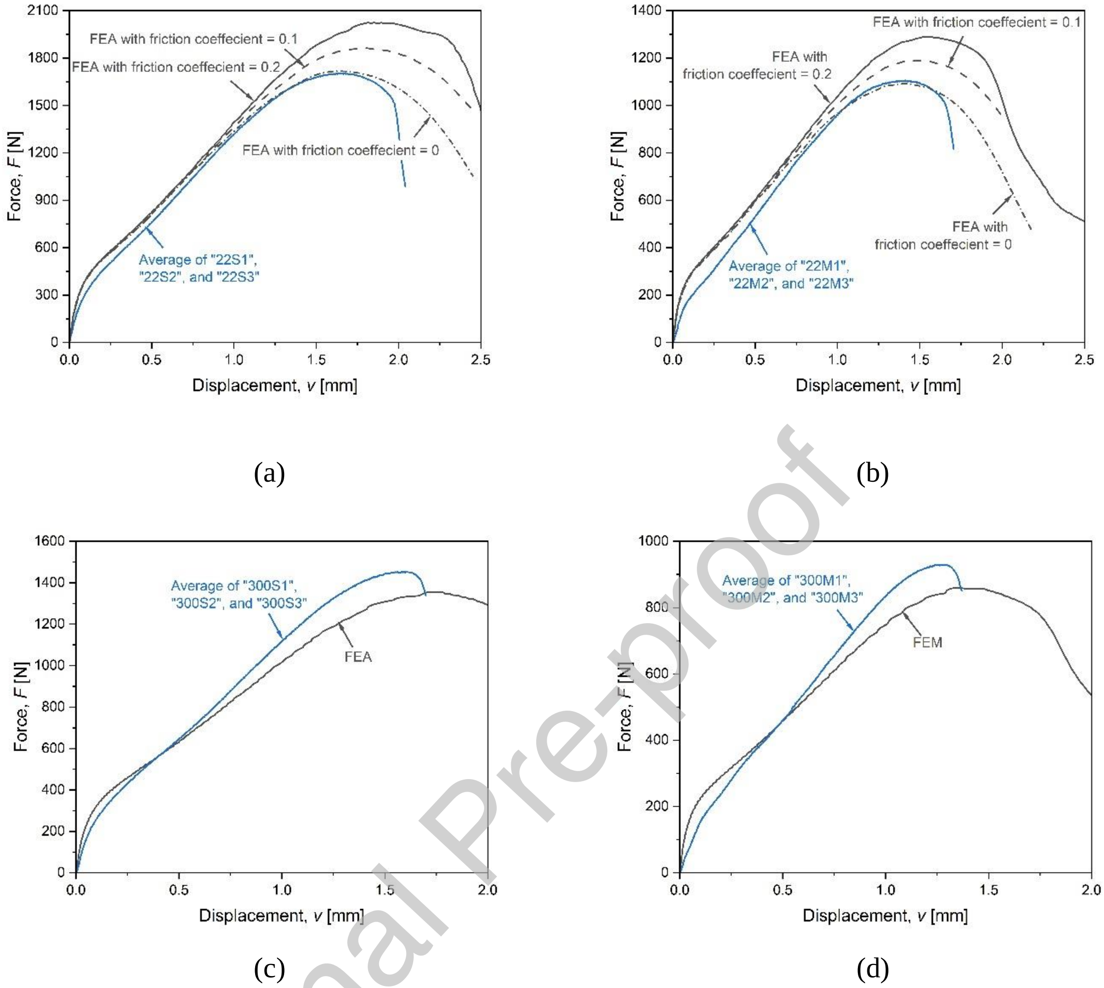

Fig. 14. Comparison between force-displacement curves from FEA and force-compliance corrected displacement curves from experiments: (a) standard Φ8 mm SPT at 22°C; (b)) Φ5.35 mm SPT at 22°C; (c)) standard Φ8 mm SPT at 300°C; (d)) Φ5.35 mm SPT at 300°C.

Fig. 14(a) and (b) shows that for 22 °C tests, the FEA predicts a force larger than the experimental response. For a displacement lower than 1 mm, the force difference remain constant around 50 N. This slight disagreement results from the different compliance induced by the discrete rigid puncher used in the FEA. In the experiment, the puncher can be seen as linear elastic rather than discrete rigid. But, beyond 1 mm displacement, the difference on the magnitude of the force gets much larger, which can be caused by the friction coefficient applied in the model. Fig. 14 (a) and (b) shows that when friction coefficient decreases, the differences between FEA and experiments also decrease and that friction only makes a difference on the predicted force when it reaches 80% of the maximum force as stated in [29]. Hence, the sudden increase of the force difference measured above 1 mm displacement can possibly be attributed to the inappropriate friction coefficient used. For 300 °C, the difference between the FEA and experimental values is smaller. The difference in maximum force may be caused by the larger thickness of the experimental specimens (0.2 mm thicker than theoretical value). However, when approaching the maximum force, the shape of the curves are not identical, the experimental curves drop suddenly while the FEA curves exhibit a gradual decrease. This may indicate that the current elastic-plastic constitutive model or hardening law adopted in the FEA is not capable of capturing the deformation processes beyond the UTS, and more advanced material models with a richer yield surface description may be needed. Further comparisons are also made between the yield stress extracted from FEA and from experiments, the results are presented in Table 9.

Table 9 Comparison between the YS and UTS extracted from FEA and experiments.

Test Type	Test Temperature [°C]	Label	UTS-Tensile [MPa]	$F_m/(h_0 v_m)$ [MPa]	UTS-SPT [MPa]	YS-Tensile [MPa]	$F_e/(h_0^2)$ [MPa]	YS-SPT [MPa]
Standard Φ8 mm	22	FEA	660	2184	646	538	1473	706
	22	EXP		2044	606		1342	643
	300	FEA	511	1541	456	444	1207	578
	300	EXP		1773	530		1038	497
Φ5.35 mm	22	FEA	660	2098	621	538	1470	704
	22	EXP		1974	584		921	441
	300	FEA	511	1587	470	444	1171	561
	300	EXP		1748	524		938	450

Table 9 shows that the UTS predictions by both FEA and experimental curves are close to one-another, with a difference within 10% at 22°C and 15% at 300°C for both SPT set-ups. However for YS, the predictions resulting from the FEA are generally less-accurate than when applying the extracting procedure directly on experimental results, with discrepancies up to 30% when compared with the tensile test results. Moreover, the SPT gives inaccurate YS, which are even larger than the UTS extracted. Same phenomenon can also be found in [32] for EUROFER 97. As is also stated in [32], the reason behind this may be that the $\beta_{Rp0.2}$ factor given in the standard is not suitable for EUROFER 97 and a re-fit of the $\beta_{Rp0.2}$ factor is needed.

5. Conclusions

In this work, a miniaturized SPT setup with a specimen diameter equals to 5.35 mm is proposed and validated through finite element modelling and experimental analyses. The specific size of 5.35 mm is driven by the need to perform irradiation screening tests and currently available SP size of 8 mm is too large to fit enough samples into one irradiation campaign and 3 mm is too small for proper labelling and remote handling of active samples. The SPT setup parameters are modified from the standardized values following Chakrabarty model and FEA optimization. A set of validation experimental tests using standard 8 mm samples, miniaturized 5.35 mm samples and uniaxial tensile tests on EUROFER97 steel are conducted to verify the applicability and reliability of the results obtained with 5.35 mm sample. The following conclusions can be drawn:

- A rigorous methodology has been followed to establish the non-standard SPT set-up. The methodology contains theoretical calculation based on Chakrabarty model and finite element analyses. Criteria are also given to determine the most suitable non-standard Small Punch test set-up.
- Based on the methodology and criteria, a new SPT rig geometry with a sample diameter of 5.35 mm, a specimen thickness of 0.4 mm, a receiving hole diameter of 3.2 mm, and a punch diameter of 2 mm has been developed and validated.
- Both the standard Φ = 8 mm and the newly-proposed Φ = 5.35 mm SPTs have a good reproducibility and are capable of capturing the dependence of material properties on test temperature in line with uniaxial tensile test results.
- Despite a degree of imprecision of up to 20% on the extraction of the yield stress and 10% on ultimate tensile strength by SPT, the scatter and accuracy of both YS and UTS calculated from both 8 and 5.35 mm SP tests are within the same order of magnitude.

- The newly-proposed Φ = 5.35 mm SPT set-up is validated and can be used for further testing including neutron irradiated samples.

Overall, the newly-proposed Φ = 5.35 mm SPT set-up shows the same level of reliability in predicting the YS and UTS as the standard Φ = 8 mm SPT configuration, and can be used for screening and qualification of irradiation exposed materials in the future. Future works will aim at a more accurate procedure to extract YS and UTS by taking bending and friction into account.

Acknowledgement:

This work has been carried out within the framework of the INNUMAT project, funded by the European Union via the Euratom Research and Training Programme 2021-2022 under the grant agreement No. 101061241. Views and opinions expressed are however those of the author(s) only and do not necessarily reflect those of the European Union or the European Commission. Neither the European Union nor the European Commission can be held responsible for them.

Appendix A. The procedure to extract YS and UTS from SPT

In order to determine YS, the tri-linear method given in the standard is used since the displacement is the measurand in this test configuration. The method relies on the assumption of a linear correlation between the tensile yield stress ($R_{p0.2}$) and the elastic-plastic transition force divided by the squared thickness. The general empirical expression of the EN standard reads:

$$R_{p0.2} = \frac{\beta_{Rp0.2} F_e}{h_0^2}, \tag{A.1}$$

where $\beta_{Rp0.2}$ is the correlation factor used for extracting YS and is given as 0.479 in the standard for standard $\Phi = 8$ mm SPT, F_e is the Elastic-plastic transition force and can be obtained as the force, f_A in the following equation. This f_A can determined through a trilinear fitting of the SPT curve in the deflection range [0, h_0]. The trilinear function is defined as:

$$f(v) = \begin{cases} 0 & for\ 0 \le v < v_0, \\ \frac{f_A}{v_A - v_0}(v - v_0) & for\ v_0 \le v < v_{A,} \\ \frac{f_B - f_A}{v_B - v_A}(v - v_A) + f_A & for\ v_A \le v \le v_{B.} \end{cases} \tag{A.2}$$

In this equation, v_B is a fixed value equal to h_0, and f_A, f_B, v_0 and v_A are all varying parameters to be optimized by minimizing the error as follows:

$$err = \int_0^{v_B} [F(v) - f(v)]^2 dv. \tag{A.3}$$

Same method is used to determine yield stress with the newly-proposed $\Phi = 5.35$ mm SPT set-up. The value of $\beta_{Rp0.2}$ is determined based on Chakrabarty model. In the Chakrabarty model, the relationships between force to stress ratio for both test geometries can be calculated and based on this, conversion ratio for force to stress ratio can be calculated and is given as:

$$\frac{\left[\frac{F}{\sigma}\right]_8}{\left[\frac{F}{\sigma}\right]_{5.35}} = 1.5625. \tag{A.4}$$

Therefore, if F in the above equation is substituted as F_e, and σ is substituted as $R_{p0.2}$, and using Eq. (A.1) to calculate $R_{p0.2}$, Eq. (A.4) can be changed into:

$$\frac{\left[\frac{F_e}{R_{p0.2}}\right]_8}{\left[\frac{F_e}{R_{p0.2}}\right]_{5.35}} = \frac{0.25 / \left[\beta_{Rp0.2}\right]_8}{0.16 / \left[\beta_{Rp0.2}\right]_{5.35}} = \frac{0.25\left[\beta_{Rp0.2}\right]_{5.35}}{0.16\left[\beta_{Rp0.2}\right]_8} = 1.5625. \quad (A.5)$$

Thus, the value of $\beta_{Rp0.2}$ for the Φ5.35 mm SPT setup is the same as standard Φ = 8 mm SPT set-up, which is 0.496. It is also important to recognize that the $\beta_{Rp0.2}$ in the standard was determined empirically from a data base of tests produced by a number of laboratories with different test-setups and of course different personnel.

The method used in this study to extract the UTS is the maximum force method described in the standard. The Ultimate Tensile Strength, R_m, as described in the standard, can be calculated as:

$$R_m = \frac{\beta_{Rm} F_m}{h_0 v_m}, \quad (A.6)$$

where F_m stands for the maximum force, v_m is the displacement at F_m, and β_{Rm} is the correlation factor used for extracting UTS. In this study, the value of β_{Rm} is not taken directly from the standard, but from an empirical equation given in [33,34]. The equation is written:

$$\frac{\beta_{Rm}}{v_m} = \frac{0.3R^{0.2}}{r^{0.2}(h+r)}, \quad (A.7)$$

where v_m is the theoretical value calculated based on the Chakrabarty model, R is the radius of receiving hole, r is the radius of the puncher, and h is the theoretical thickness of the sample. Based on the equation, it can be calculated that for both standard Φ = 8 mm sample and newly-proposed Φ = 5.35 mm sample, the value of the correlation factor is the same, which is 0.296. Please note that the value of β_{Rm} here is a specific theoretical value for the ideal sample that has the thickness of 0.5 mm or 0.4 mm. For the specimens tested in this study, a correction on β_{Rm} based on the actual thickness is conducted. Based on the Chakrabarty membrane stretch model, the value of β_{Rm} is directly proportional to (1+h/r). In this context, it is important to note that the Chakrabarty equations do not take friction and bending into account which has been shown to impact the location of the v_m. The correction is made as follow:

$$\frac{\beta_{Rm-th}}{\beta_{Rm}} = \frac{\left(1 + \frac{h_{th}}{r}\right)}{\left(1 + \frac{h_0}{r}\right)}, \quad (A.8)$$

where, the $\beta_{Rm\text{-}th}$ stands for the theoretical value of β_{Rm}, which is 0.296, β_{Rm} stands for the value after thickness correction, h_{th} is the theoretical thickness, which is equal to 0.5 mm for standard Φ = 8 mm SPT and 0.4 mm for newly-proposed Φ = 5.35 mm SPT, h_0 is the average thickness of the sample, and r is the punch radius.

References

[1] N. Holtkamp, An overview of the ITER project, Fusion Eng. Des. 82 (2007) 427–434. https://doi.org/10.1016/j.fusengdes.2007.03.029.

[2] N. Holtkamp, The status of the ITER design, Fusion Eng. Des. 84 (2009) 98–105. https://doi.org/10.1016/j.fusengdes.2008.12.119.

[3] G. Federici, R. Kemp, D. Ward, C. Bachmann, T. Franke, S. Gonzalez, C. Lowry, M. Gadomska, J. Harman, B. Meszaros, C. Morlock, F. Romanelli, R. Wenninger, Overview of EU DEMO design and R&D activities, Fusion Eng. Des. 89 (2014) 882–889. https://doi.org/10.1016/j.fusengdes.2014.01.070.

[4] G. Federici, C. Bachmann, W. Biel, L. Boccaccini, F. Cismondi, S. Ciattaglia, M. Coleman, C. Day, E. Diegele, T. Franke, M. Grattarola, H. Hurzlmeier, A. Ibarra, A. Loving, F. Maviglia, B. Meszaros, C. Morlock, M. Rieth, M. Shannon, N. Taylor, M.Q. Tran, J.H. You, R. Wenninger, L. Zani, Overview of the design approach and prioritization of R&D activities towards an EU DEMO, Fusion Eng. Des. 109–111 (2016) 1464–1474. https://doi.org/10.1016/j.fusengdes.2015.11.050.

[5] RCC-MRx, Design, Construction rules for mechanical components of nuclear installations: high temperature, research and fusion reactors, AFCEN (2022).

[6] G. Pintsuk, E. Diegele, S.L. Dudarev, M. Gorley, J. Henry, J. Reiser, M. Rieth, European materials development: Results and perspective, Fusion Eng. Des. 146 (2019) 1300–1307. https://doi.org/10.1016/j.fusengdes.2019.02.063

[7] C. Cabet, F. Dalle, E. Gaganidze, J. Henry, H. Tanigawa, Ferritic-martensitic steels for fission and fusion applications, J. Nucl. Mat. 523 (2019) 510–537. https://doi.org/10.1016/j.jnucmat.2019.05.058.

[8] Innovative Structural Materials for Fission and Fusion (INNUMAT). https://ec.europa.eu/info/funding-tenders/opportunities/portal/screen/how-to-participate/org-details/999999999/project/101061241/program/43298916/details (accessed July 1, 2024).

[9] X. Chen, A. Bhattacharya, M.A. Sokolov, L.N. Clowers, Y. Yamamoto, T. Graening, K.D. Linton, Y. Katoh, M. Rieth, Mechanical properties and microstructure characterization of Eurofer97 steel variants in EUROfusion program, Fusion Eng. Des. 146 (2019) 2227–2232. https://doi.org/10.1016/j.fusengdes.2019.03.158.

[10] O. Kachko, A. Puype, D. Terentyev, G. Bonny, W. Van Renterghem, R.H. Petrov, Development of RAFM steels for high temperature applications guided by thermodynamic modelling, Nucl. Mater. Ener. 32 (2022) 101211. https://doi.org/10.1016/j.nme.2022.101211.

[11] L. Tan, L.L. Snead, Y. Katoh, Development of new generation reduced activation ferritic-martensitic steels for advanced fusion reactors, J. Nucl. Mat. 478 (2016) 42–49. https://doi.org/10.1016/j.jnucmat.2016.05.037.

[12] E. Materna-Morris, R. Lindau, H.C. Schneider, A. Möslang, Tensile behavior of EUROFER ODS steel after neutron irradiation up to 16.3 dpa between 250 and 450 °C, Fusion Eng. Des. 98–99 (2015) 2038–2041. https://doi.org/10.1016/j.fusengdes.2015.07.015.

[13] G.E. Lucas, Review of small specimen test techniques for irradiation testing, Metall. Trans. A 21 (1990) 1105–1119. https://doi.org/10.1007/BF02656531.

[14] P. Hosemann, C. Shin, D. Kiener, Small scale mechanical testing of irradiated materials, J Mater. Res. 30 (2015) 1231–1245. https://doi.org/10.1557/jmr.2015.26.

[15] ASTM International, ASTM E3205-20 Standard Test Method for Small Punch Testing of Metallic Materials, 2020. West Conshohocken, PA. https://doi.org/10.1520/E3205-20.

[16] British Standards Institution, BS EN 10371-2021; Metallic Materials—Small Punch Test Method, 2021. London, UK.

[17] R. Lancaster, G. Davies, H. Illsley, S. Jeffs, G. Baxter, Structural integrity of an electron beam melted titanium alloy, Materials 9 (2016) 470. https://doi.org/10.3390/ma9060470.

[18] S. Arunkumar, Overview of small punch test, Met. Mater. Int. 26 (2020) 719–738. https://doi.org/10.1007/s12540-019-00454-5

[19] X. Jia, Y. Dai, Small punch tests on martensitic/ferritic steels F82H, T91 and Optimax-A irradiated in SINQ Target-3, J. Nucl. Mat. 323 (2003) 360–367. https://doi.org/10.1016/j.jnucmat.2003.08.018.

[20] E. Altstadt, F. Bergner, M. Houska, Use of the small punch test for the estimation of ductile-to-brittle transition temperature shift of irradiated steels, Nucl. Mater. Ener. 26 (2021) 100918. https://doi.org/10.1016/j.nme.2021.100918.

[21] C.F. Yao, Y. Dai, DBTT shift of Optifer-IX, Eurofer 97 and MA956 steels after irradiation evaluated with small punch tests, J. Nucl. Mat. 544 (2021) 152725. https://doi.org/10.1016/j.jnucmat.2020.152725.

[22] S.H. Song, R.G. Faulkner, P.E.J. Flewitt, P. Marmy, L.Q. Weng, Small punch test evaluation of neutron-irradiation-induced embrittlement of a Cr–Mo low-alloy steel, Mater. Charact. 53 (2004) 35–41. https://doi.org/10.1016/j.matchar.2004.07.006.

[23] E. Altstadt, H.E. Ge, V. Kuksenko, M. Serrano, M. Houska, M. Lasan, M. Bruchhausen, J.M. Lapetite, Y. Dai, Critical evaluation of the small punch test as a screening procedure for mechanical properties, J. Nucl. Mat. 472 (2016) 186–195. https://doi.org/10.1016/j.jnucmat.2015.07.029.

[24] S.H. Song, R.G. Faulkner, P.E.J. Flewitt, P. Marmy, L.Q. Weng, Small punch test evaluation of neutron-irradiation-induced embrittlement of a Cr–Mo low-alloy steel, Mater. Charact. 53 (2004) 35–41. https://doi.org/10.1016/j.matchar.2004.07.006.

[25] Y. Snir, D. Moreno, I. Silverman, S. Samuha, Y. Eisen, D. Eliezer, Y. Gelbstein, S. Haroush, Mechanical properties of proton bombarded SS316L thin foils using the small punch technique, J. Nucl. Mat. 540 (2020) 152340. https://doi.org/10.1016/j.jnucmat.2020.152340.

[26] S. Piela, R. Howard, A. Le Coq, K. Linton, J. Li, Design and Assembly of Rabbit Capsules for Irradiation of Prototype Metal and Nanocomposite Specimens in the High Flux Isotope Reactor, ORNL/SPR-2019/1306, Oak Ridge, TN (2019).

[27] J. Chakrabarty, A theory of stretch forming over hemispherical punch heads, Int. J. Mech. Sci. 12 (1970) 315–325. https://doi.org/10.1016/0020-7403(70)90085-8.

[28] Dassault, ABAQUS/Standard User's Manual, (2024). https://www.3ds.com/products-services/simulia/products/abaqus/.

[29] I. Simonovski, S. Holmström, M. Bruchhausen, Small punch tensile testing of curved specimens: Finite element analysis and experiment, Int. J. Mech. Sci. 120 (2017) 204–213. https://doi.org/10.1016/j.ijmecsci.2016.11.029.

[30] C.C. Chang, D. Terentyev, A. Bakaev, A. Zinovev, D. Del Serra, P. Verleysen, T. Pardoen, On the equivalence of mini-flat and cylindrical tensile geometries to extract hardening law and ductility of Eurofer97, Fusion Eng. Des.194 (2023) 113717. https://doi.org/10.1016/j.fusengdes.2023.113717.

[31] ASTM International, ASTM E8/E8M-16a Standard Test Methods for Tension Testing of Metallic Materials, 2016. West Conshohocken, PA. https://doi.org/ 10.1520/E0008_E0008M-16A.

[32] T. Melkior, D. Terentyev, C.C. Chang, A. Bakaev, S. Holmström, S. Lebediev, A. Paputsia, Mechanical properties of structural metallic alloys for nuclear applications deduced by small punch test, J. Nucl. Mat. 583 (2023) 154521. https://doi.org/10.1016/j.jnucmat.2023.154521.

[33] B. Holmstrom, I. Simonovski, S. Ripplinger, E. Altstadt, R. Delville, M. Serrano, V. Radu, Tensile and creep property determination of 15-15Ti fuel cladding steel by small punch testing, International Conference on Life Management and Maintenance for Power Plants, (2016) 293-305.

[34] European Committee for Standardization, CWA 15627 Small punch test method for metallic material, 2006. Brussels, Belgium.

Declaration of interests

☒ The authors declare that they have no known competing financial interests or personal relationships that could have appeared to influence the work reported in this paper.

☐ The authors declare the following financial interests/personal relationships which may be considered as potential competing interests: